NONLINEAR CYCLIC BEHAVIOR OF REINFORCED CONCRETE PLANE STRESS MEMBERS

Haluk Aktan[I] and Movses J. Kaldjian[II]

SUMMARY

A finite element model made of two individual parts is developed to describe separately the linear and the nonlinear properties of a material. The linear behavior of each region is defined by an elastic plane stress element and its nonlinear behavior is provided by inserting a joint element connected to a boundary of the region. The stiffness matrix of the combined element is obtained from properties of concrete and orthogonally placed reinforcing steel. Four hysteretic stress-strain relationships are developed. The cyclic behavior of concrete under normal stresses is described by an enveloping parabola from zero to ultimate stress, and a straight line the rest of the way to the crushing strain. The shear stiffness is assumed to be a function of normal stiffness for the uncracked state of concrete. The cyclic behavior of reinforcing steel is described by a simple bi-linear model, but after the crushing of concrete a new hysteretic relationship is defined which allows the reinforcing steel to buckle in compression. The applicability of the model is demonstrated by working out two examples of slender shear walls, and comparing the results with the PCA experiments.

FINITE ELEMENT MODEL

The displacement of a finite element plane stress member is considered to consist of a linearly elastic part and a nonlinear part. The member is divided into subregions and the respective behavior of these subregions are described by two different types of elements. Constant stress triangles are used to represent linearly elastic behavior and special boundary elements between adjacent joints, to express nonlinearity of each subregion. The boundary or joint elements are line elements with zero initial width they connect the linearly elastic subregions and account for the nonlinearities in the system.

The stiffness matrices for the elements are derived from the assumption that concrete with reinforcing steel forms a composite material. Two orthogonal reinforcing steel directions are assumed and the composite material property matrix is formed by using strain compatibility as follows

$$\{\sigma\}_{concrete} = [D]_{concrete} \{\varepsilon\} \quad (1)$$

$$\{\sigma\}_{steel} = [D]_{steel} \{\varepsilon\} \quad (2)$$

where $\{\sigma\}$ is the stress vector, $[D]$ is the material property matrix, $\{\varepsilon\}$ is the strain vector and

$$[D]_{Total} = [D]_{concrete} + [D]_{steel} \quad (3)$$

(I) Systems Analyst, Ph.D.'77, Ann Arbor Computer Corp., Ann Arbor, MI.,48104
(II) Professor, Depts. of Civil Engr. and Naval Arch., University of Michigan, Ann Arbor, MI., 48109

The exploded view of a subregion and the placement of the corresponding joint element is show in Figure 1. The nodes of the joint element are defined by (i,j,k,l) and each node has two displacement components, Δu in X-direction, Δv in Y-direction respectively.

The strains in the joint elements (l,j,k,l), shown in Figure 1. are the nonlinear strains of the subregion (i,j,m,p). The elastic strains are computed from the displacements of the nodes (m,p,k,l). The joint strain-displacement relations are obtained by subtracting the elastic strains of the constant stress triangle from the total strains of the subregion.

The stress-strain relationship for the joint element is defined in two directions namely σ_n, ε_n for normal, and σ_s, ε_s for shear. The material property matrix relating the stresses to the strains is

$$\begin{Bmatrix} \sigma_s \\ \sigma_n \end{Bmatrix} = \begin{bmatrix} k_{ss} & k_{ns} \\ k_{sn} & k_{nn} \end{bmatrix} \begin{Bmatrix} \varepsilon_s \\ \varepsilon_n \end{Bmatrix} \qquad (4)$$

Due to symmetry of material properties, k_{sn} and k_{ns} are equal, thus,only 3 terms of the equation (4) need to be defined. The terms of the composite material property matrix for reinforced concrete with reinforcing steel located parallel to X and Y coordinate directions (Figure 1) are derived as

$$\begin{aligned} k_{ss} &= G + E_s \sin^2\theta . \cos^2\theta (l_x + l_y) \\ k_{nn} &= E_c + E_s (l_x . \cos^4\theta + l_y \sin^4\theta) \\ k_{ns} &= E_s (l_x . \cos^3\theta . \sin\theta - l_y \cos\theta \sin^3\theta) \end{aligned} \qquad (5)$$

where E_c, E_s and G are elastic modulus of concrete and steel, and shear modulus of concrete respectively, l_x and l_y are the ratio of steel area to the unit concrete area placed parallel to X and Y directions respectively. For a detailed discussion of the stiffness matrix of this joint element see Reference (1).

The initial global stiffness matrix is formed in two matrices using virgin material properties. The first matrix contains the stiffness contribution of the constant stress triangular elements and the second matrix contains the stiffness contributed by joint elements. The stiffness of the joint element is derived for incremental displacements between the nodes of the upper and the lower subregions.

The triangular elements are kept linearly elastic throughout the loading, thus, the matrix of triangular elements is generated only once. The joint element stiffnesses are regenerated at every loading step to follow the nonlinear behavior. The strains of the joint elements are evaluated from the relative displacement between the nodes. The shearing and the normal stresses are computed using the appropriate hyteresis laws. The nodal forces on the joint element are calculated from the element stresses and the residual forces are redistributed to the system during the next incremental loading step. An iterative approach to redistribute the residual forces is possible if, on the same loading step a zero value is assigned for the next

load increment.

MATERIAL MODELS

The material models developed are based on extensive experimental work by earlier investigators. (3,4,5,6). The material properties defined for the analytical procedure are: tangent modulus of concrete (E_c), shear modulus of concrete (G), and the elastic modulus of steel (E_s). The models derived to define these parameters are for normal stress behavior of concrete, for shear transmission across cracked concrete, and for reinforcing steel both before and after crushing of concrete.

The model developed to approximate the cyclic behavior of concrete under normal stresses is shown in Figure 2. The envelope curve is described by Hoegnestad's parabola from zero to ultimate strain and by a straight line from ultimate to crushing strain. The terminology for the definition of the loading and unloading curves (plastic strain ratio, stability limit and common point) are adopted from Reference (3).

Unloading starts from the envelope when the strains start decreasing while the concrete is under compression. The unloading curve is constructed by two linear segments. The initial slope of the unloading curve, AB in Figure 3(a), is taken equal to the initial elastic stiffness of concrete $.012\ f'_c/\varepsilon_{cu}$ (N/mm^2). Before constructing the second branch of the unloading curve, BC in Figure 3(a), the first branch of the reloading curve, DE in Figure 3(a) is defined. The plastic strain ratio, point D in Figure 3(a), is computed from the formula:

$$\frac{\varepsilon_n}{\varepsilon_{cu}} = 0.145\frac{\varepsilon_e}{\varepsilon_{cu}} + 0.130\left(\frac{\varepsilon_e}{\varepsilon_{cu}}\right)^2 \qquad (6)$$

where, ε_n and ε_e are the plastic and envelope strains and ε_{cu} is the strain in concrete at ultimate stress.

Point E in Figure 3(a) is defined as the stability limit. The equations defining the locations of the stability limit are adopted from Reference (3) with a change in the coefficients so that they are valid for the envelope curve used in this study. Points D and E define the first branch of the reloading curve DE. The second branch of the reloading curve, BC, is constructed parallel to DE. It is a straight line between the stability limit and the envelope curve at a point where the envelope strain is 10% larger than the pervious unloading envelope strain.

If a full unloading cycle from the envelope to zero strain is not achieved, different paths for unloading and reloading curves are defined. If the stresses are cycled between zero and the stability limit the unloading curve follows branch DE and there is no energy dissipation. Cycles of maximum stress between the stability limit and the common point dissipate energy but do not create additional permanent strain (Figure 3(a)). If the maximum stress reaches a point above the common point and unloading starts prior to reaching the envelope curve, a projection of that unloading point onto the envelope, A" in Figure 3(b), is used to compute the new plastic strain. In the case where reloading starts prior to total release of

stress, the reloading curve follows the path $C' D' E' F A''$ in Figure 3(c). The point D' is located such that $CD/C'D' = BC/BC'$.

For cycles between strain limits of $0.4\varepsilon_{cu}$ to $1.6\varepsilon_{cu}$ the analytical model results match well with the experiment, but for unloading strain less than $0.4\varepsilon_{cu}$ the model dissipates less energy and for unloading strains higher than $1.6\varepsilon_{cu}$ dissipates more energy than the experimental results.

The hysteretic model representing the shear transfer across a crack is described by four linear branches (Figure 4). The initial slip observed in experiments (4) is defined by a low stiffness region branch 1. With increasing slip the material gains stiffness as branch 2 is reached. Unloading follows branch 3 until zero stress and the slip axis is defined to be the fourth branch. The unloading curve, branch 4, follows the zero stress axis until zero strain is reached then the element starts to gain stiffness in the reverse direction. The turning point, where the stiffness begins to increase, is taken as a function of the crack width. The increase in crack width during a cycle is handled by defining a new hysteresis for that crack width. If there is a decrease in crack width the hysteresis relationship is assumed to follow the path generated by the previous larger crack width.

The cracks start to close when the loads on the system are reduced. After a crack closes the full shear stiffness transmission capacity of concrete is not regained, it is assumed to be proportional to the normal stress on the closed crack. The initial stiffness for the closed crack case is taken equal to the loading branch D (Figure 4) to satisfy the compatibility of shear stiffness during transition.

A simple bilinear model is assumed to represent the stress-strain hysteresis of reinforcing steel. Strain reversals are assumed to have a slope defined by the initial elastic modulus. The strain hardening branches envelope the loading unloading segments. Initial elastic modulus, yield stress, strain hardening slope and the rapture strain are used to construct the hysteretic relationship for steel. In the tensile directions the reinforcing steel follows the bilinear hysterisis although the concrete might crack. The compressive part of the hysterisis can only be achieved when the steel is supported by concrete around it. When the concrete crushes under compression and the steel has not ruptured, a new hysteresis relation is defined, which allows the reinforcing steel to buckle in compression (Figure 5).

EXAMPLES

To demonstrate the usefulness of the proposed analytical procedure two selected experiments (monotonically loaded and cyclically loaded) on slender shear walls are analyzed and compared with experimental data (7,8).

To model the shear wall for analysis, the dimensions and the finite element mesh were defined first. The damage to the experimental walls were concentrated within a small distance from the base when compared with the overall height of the wall (which is the case in most slender shear walls). The monotonically loaded model had a height of 270cm, depth of 190cm, and thickness of 7.5 cm. The corresponding dimensions for the cyclically loaded model were 225cm, 190cm and 10cm respectively. Comparison of the experimental and analytical models is shown in Figure 6.

Horizontal reinforcement consisted of 3% of the gross concrete area evenly distributed along the depth and the height of the walls. A comparison of the analytical moment-curvature and experimental moment curvature for the monotonically loaded model is shown in Figure 7. The analytical curvature was computed in a manner similar to the experimental curvature, but over a 9cm gage. length. This length was based upon the location of the joint elements in the analytical model. There is good agreement between the experimental and analytical results as seen in Fig. 7.

The cyclically loaded specimen was designed in accordance with the ACI 318-71 code. The vertical reinforcement was concentrated within the outside tenths of the width of the wall. The nominal web reinforcement was 0.25% of the gross concrete area. The shear reinforcement was 0.19% on the outside tenths of the width and 0.16% on the web. The specimen was loaded like a vertical cantilever with concentrated forces at the top through a slab. The loads were alternated for 30 cycles. The first ten cycles were all below the yield reflection with corresponding forces between 35kN and 67kN. The joint elements were placed along expected crack locations and maximum stress directions. The model had 95 subregions with joint elements. It included 28 independent and 210 incremental displacement components. Application of the first nine cycles of load to the model did not produce any significant amount of inelastic response even though some loss in stiffness was observed. Because of computation cost it was considered to be impractical to reload the analytical model for the first nine cycles. To have a basis of comparison in the cyclic loading example, the concrete properties were changed to represent the effects of the first nine cycles of loading. Although this will not be directly valid for comparing the load displacement results, it was important to find out if the analytical model was capable to represent the general characteristics of a cyclically loaded reinforced concrete shear wall.

The comparison of the analytical and experimental moment curvature results are shown in Figure 8. The analytical curvature is computed by dividing the rotation of the section 9.3cm from the base by the distance to the base 9.3cm. The experimental curvature was measured over a 7.6cm gage near the base. During the analytical study of the cyclic behavior of the wall 64 loading increments were applied and iterations at 20 load levels were performed. The maximum number of iterations per load level was limited to 5. This number of iterations was sufficient to decay the residual forces to a tenth of the applied maximum nodal load in almost all cases considered.

In conclusion the proposed model gave exceptionally good corrolation with monotonic test results. Although a similar claim cannot be made for the cyclic loading experiment, the overall moment-curvature behavior of the analytical model showed typical reinforced concrete shear wall characteristic behavior. Futher work is being conducted at present to improve the mathematical model and remedy this deficiency.

ACKNOWLEDGEMENT

The authors would like to thank Prof. Robert Hanson for his involvement and support in this study.

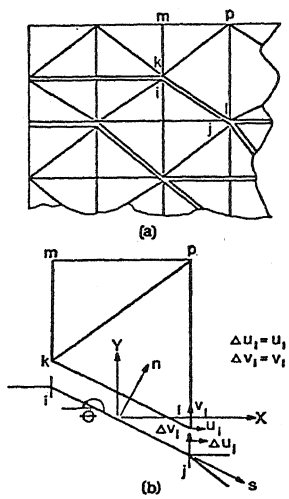

Fig. 1. (a) Partial view of 2/D F.E. model
(b) Exploded view of a region

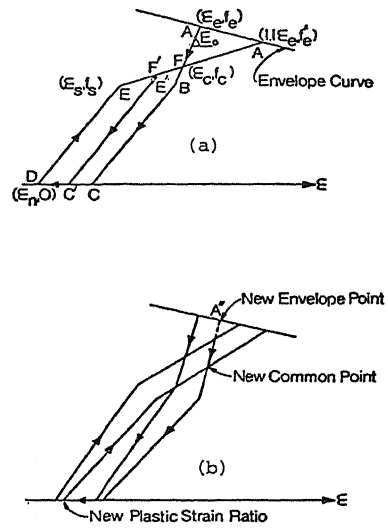

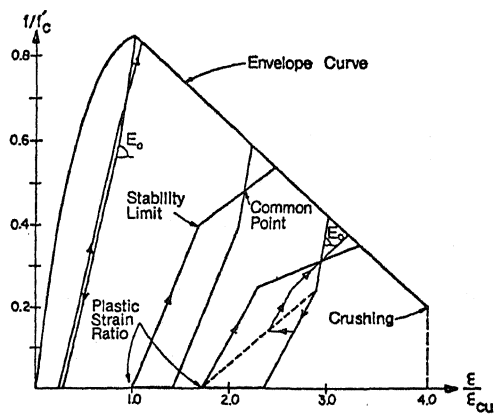

Fig. 2. Proposed model for normal behavior of concrete under cyclic stress.

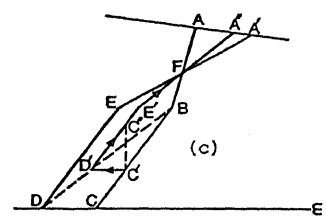

Fig. 3. (a) Unloading between the common point and the stability limit.
(b) Unloading between the common point and the envelope curve.
(c) Reloading prior to total release of stress.

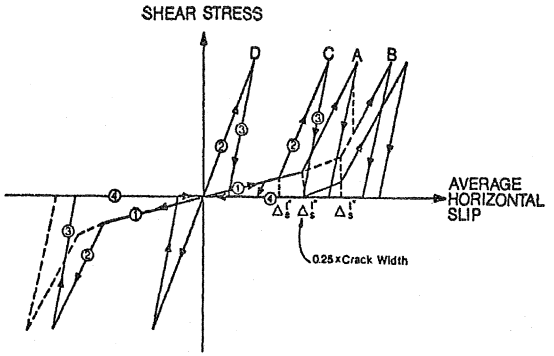

Fig. 4. Proposed model for shear transfer across the crack under cyclic shear stress.

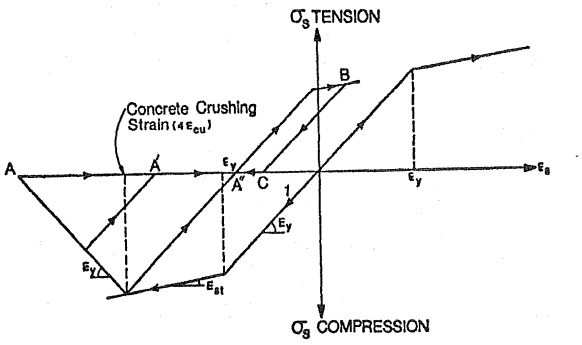

Fig. 5. Model for hysteratic behavior of reinforcing steel after crushing of concrete.

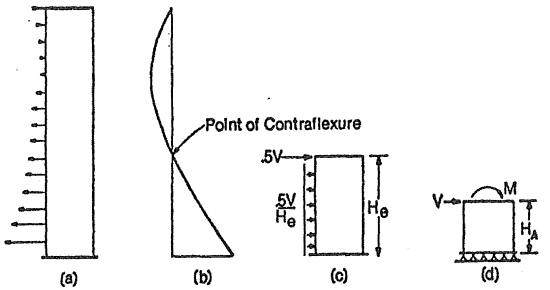

Fig. 6. (a) Forces acting on a slender shear wall, (b) Moment diagram, (c) Experimental model, (d) Analytical model.

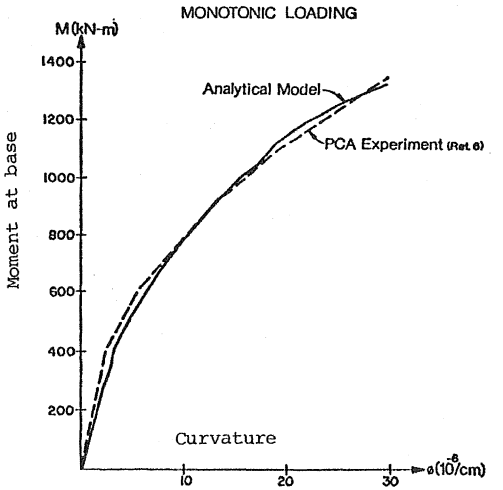

Fig. 7. Comparison of analytical and experimental moment results for monotonically loaded slender shear wall.

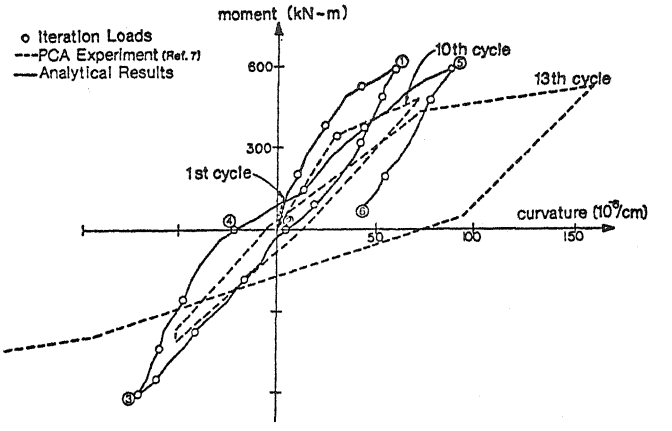

Fig. 8. Analytical and experimental moment - curvature results compared for the slender shear wall under cyclic loading.

REFERENCES

1. AKTAN, M.H. "A Method to Analyze the Cyclic Behavior of the Slender Reinforced Concrete Shear Walls" Ph.D. Thesis, University of Michigan, UMEE 77R2, Ann Arbor 1977.

2. KALDJIAN, M.J., "Composite and Layered Beams with Non-Linear Connectors," Proc. ASCE Specialty Conf. on Metal Structures, Columbia, Missouri, (Engin.Extension Series 15), June 1970

3. KARSAN, I.D. and JIRSA, J.O.,"Behavior of Concrete Under Compressive loading" Journal of the Structural Division, ASCE, Vol. 95, No.ST12, Dec. 1969, pp.2543-2563.

4. HOUDE, J. and MIRZA, M.S., "Investigation of Shear Transfer Across Cracks by Aggregate Interlock" Ecole Polytechnique de Montreal, No. 72-065, Aug. 1972.

5. GERGELY, P., STANTON, J.F. and WHITE, R.N. "Behavior of Cracked Concrete Nuclear Containment Vessels During Earthquakes," Proc. of U.S. National Conference on Earthquake Engineering, Ann Arbor, June 1975, EERJ, pp.512-518.

6. AKTAN, A.E., KARLSON, V.J. and SOZEN, M.A., "Stress-Strain Relationship of Reinforcing Bars Subjected to Large Strain Reversals," SRS Report No. 397, University of Illinois, Urbana, JUNE 1973.

7. CARDENAS, A.E. and MAGURA, D.D. "Strength of High Rise Shear Walls-Retangular Cross-Section," PCA Research Development Bulletin. RD029.01D, 1973.

8. PCA, "Structural Walls in Earthquake Resistance Structures," Experimental Program Progress Report, AUG. 1975.